

Machine Learning of coarse-grained Molecular Dynamics Force Fields

Jiang Wang,¹ Christoph Wehmeyer,² Frank Noé,^{1,2, a)} and Cecilia Clementi^{1,2, b)}

¹⁾*Rice University, Center for Theoretical Biological Physics and Department of Chemistry, Houston, Texas 77005, United States*

²⁾*Freie Universität Berlin, Department of Mathematics and Computer Science, Arnimallee 6, 14195 Berlin, Germany*

(Dated:)

Atomistic or ab-initio molecular dynamics simulations are widely used to predict thermodynamics and kinetics and relate them to molecular structure. A common approach to go beyond the time- and lengthscales accessible with such computationally expensive simulations is the definition of coarse-grained molecular models. Existing coarse-graining approaches define an effective interaction potential to match defined properties of high-resolution models or experimental data. In this paper we reformulate coarse-graining as a supervised machine learning problem. We use statistical learning theory to decompose the coarse-graining error and cross-validation to select to compare the performance of different models. We introduce CGnets, a deep learning approach, that learn coarse-grained free energy functions and can be trained by the force matching scheme. CGnets maintain all physically relevant invariances and allow to incorporate prior physics knowledge to avoid sampling of unphysical structures. We demonstrate that CGnets outperform the results of classical coarse-graining methods, as they are able to capture the multi-body terms that emerge from the dimensionality reduction.

I. INTRODUCTION

Recent technological and methodological advances have made possible to simulate macromolecular systems on biologically relevant timescales^{1–3}. For instance, we can simulate binding, folding and conformation changes of small to intermediate-size proteins on timescales of milliseconds, seconds or beyond^{4–8}. However, the extensive sampling of large macromolecular complexes on biological timescales at atomistic resolution is still out of reach. For this reason the design of simplified, yet predictive models is of great interest^{9–11}, in particular to interpret the experimental data that are becoming increasingly accessible in high throughput and resolution. Experimental data provide a partial view of certain aspects of a macromolecular system but do not directly give a full dynamical representation and simulation can help obtain a more comprehensive understanding^{12–14}. As it is clear that not every single atom is important in determining the relevant collective features of biomolecular dynamics and function, simplified models could provide more insights on the general physicochemical principles regulating biophysical systems at the molecular level. Here we use recent advances in machine

learning to design optimal reduced models to reproduce the equilibrium thermodynamics of a macromolecule.

Significant effort has been devoted in the last few years to apply machine learning (e.g., deep neural network or kernel methods) to learn effective models from detailed simulations^{15–19}, and specifically to learn potential energy surfaces from quantum mechanical calculations on small molecules^{20–35}. In principle a similar philosophy could be used to define models at lower resolutions, that is to learn the effective potential energy of coarse-grained (CG) models from fine-grained (e.g., atomistic) molecular dynamics (MD) simulation data^{36,37}.

There are however important differences. In the definition of potential energy surfaces from quantum calculations, the relevant quantity to reproduce is the energy, and it is relatively straightforward to design a loss function for a neural network to minimize the difference between the quantum mechanical and classical energy (and forces^{25,33}) over a sample of configurations. In contrast, in the definition of a CG model, it is important to define what are the properties of the system that need to be preserved by the coarse-graining.

Several approaches have been proposed to design effective CG energy functions for large molecular systems that either reproduce structural features of atomistic models (bottom-up)^{38–43} or reproduce macroscopic properties for one or a range of systems (top-down)^{12–14,44–47}. Popular bottom-up ap-

^{a)}Electronic mail: frank.no@fu-berlin.de

^{b)}Electronic mail: cecilia@rice.edu

proaches choose that the CG model reproduce the canonical configuration distribution determined by the atomistic model. For instance, one may want to be able to represent the different metastable states populated by a protein undergoing large conformational changes. One of the difficulties in the practical application of these methods has been that, in general, a CG potential optimally reproducing selected properties of a macromolecular system includes many-body terms that are not easily modeled in the energy functions.

In this paper we formulate the well-known force matching procedure for coarse-graining as a supervised machine learning problem. Previously, coarse-graining has been mostly discussed as a fitting procedure, but the aim of machine learning is to find a model that has minimal prediction error on data not used for the training. We use classical statistical learning theory to show that the force matching error can be decomposed into Bias, Variance and Noise terms and explain their physical meaning. We also show that the different CG models can be ranked using their cross-validation score.

Second, we discuss a class of neural networks for coarse-graining molecular systems, CGnets. CGnets have a lot of similarities with neural networks used to learn potential energy surfaces from quantum data, for instance they have the relevant invariances (e.g., rotational and translational invariance of the predicted energy, equivariance of the predicted force). In contrast to potential energy networks, CGnets predict a free energy (potential of mean force) and then use the gradient of this free energy with respect to the input coordinates to compute a mean force on the CG coordinates. As the CG free energy is not known initially, only the force information can be used to train the network.

Third, CGnets are extended to regularized CGnets. Using a generic function approximator such as a neural network to fit the CG force field from training data only may lead in force predictions that are “catastrophically wrong” for configurations not captured by the training data, i.e., predictions of forces in the direction of increasingly unphysical states that lead to diverging and unrealistic simulation results. We address this problem by adding a prior energy to the free energy network that does not compromise the model accuracy within the training data region, but ensures that the free energy approaches infinity for unphysical states, resulting in a restoring force towards physically meaningful states.

Finally, we demonstrate that CGnets succeed in learning the CG mean force and the CG free energy for a 2D toy model and for the coarse-graining of an all-atom explicit-solvent simulation of alanine

dipeptide to a CG model with 5 particles and no solvent. We show explicitly that CGnets achieve a systematically better performance than classical CG approaches which construct the CG free energy as a sum of few-body terms. The inherently multi-body CGnet energy function can represent free energy minima that are not captured by a few-body spline model, highlighting the importance of machine learning and generic function approximators in the CG problem.

II. THEORY AND METHODS

Here we introduce the main theoretical concepts and define the machine learning problems involved in coarse-graining using the force matching principle, and introduce CGnets and regularized CGnets. The more practically inclined reader may skip to Section IID.

A. Coarse-graining with thermodynamic consistency

We first define what we mean by coarse-graining and which physical properties shall be preserved in the coarse-grained model.

The starting point in the design of a molecular model with resolution coarser than atomistic is the definition of the variables. The choice of the coarse coordinates is usually made by replacing a group of atoms by one effective particle. Because of the modularity of a protein backbone or a DNA molecule, popular models coarse-grain a macromolecule to a few interaction sites per residue or nucleotide, e.g., the C_α and C_β atoms for a protein^{44,47–49}. Alternative schemes have also been proposed for the partitioning of the atoms into coarse-grained coordinates^{50,51}. In general, given a high-dimensional atomistic representation of the system $\mathbf{r} \in \mathbb{R}^{3N}$, a CG representation is given by a coordinate transformation to a lower-dimensional space:

$$\mathbf{x} = \xi(\mathbf{r}) \in \mathbb{R}^{3n} \quad (1)$$

with $n < N$. Here we assume that ξ is linear, i.e. there is some coarse-graining matrix $\Xi \in \mathbb{R}^{3n \times 3N}$ that clusters atoms to coarse-grained beads: $\mathbf{x} = \Xi \mathbf{r}$.

The aim is to learn a coarse-grained energy function $U(\mathbf{x}; \boldsymbol{\theta})$ that will be used in conjunction with a dynamical model, e.g., Langevin dynamics, to simulate the CG molecule. $\boldsymbol{\theta}$ are the parameters of the coarse-grained model – in classical CG approaches these are parameters of the potential energy function, such as

force constants and partial charges, while here they denote the weights of the neural network.

A common objective in coarse-graining methods is to preserve the equilibrium distribution, i.e. the equilibrium distribution of the coarse-grained model shall be as close as possible to the equilibrium distribution of the atomistic model when mapped to the CG coordinates. We will be using a simulation algorithm for the dynamics such that the system's equilibrium distribution is identical to the Boltzmann distribution of the employed potential U ; therefore this objective can be achieved by enforcing the thermodynamic consistency:

$$U(\mathbf{x}; \boldsymbol{\theta}) \equiv -\frac{1}{k_B T} \ln p^{CG}(\mathbf{x}) + \text{const}, \quad (2)$$

where $k_B T$ is the thermal energy with Boltzmann constant k_B and temperature T , and the probability distribution $p^{CG}(\mathbf{x})$ is the equilibrium distribution of the atomistic model, mapped to the CG coordinates:

$$p^{CG}(\mathbf{x}) = \frac{\int \mu(\mathbf{r}) \delta(\mathbf{x} - \xi(\mathbf{r})) d\mathbf{r}}{\int \mu(\mathbf{r}) d\mathbf{r}} \quad (3)$$

and $\mu(\mathbf{r}) = \exp(-V(\mathbf{r})/k_B T)$ is the Boltzmann weight associated with the atomistic energy model $V(\mathbf{r})$. Note that the additive constant in (2) can be chosen arbitrarily. Therefore this constant will be omitted in the expressions below, which means that it will absorb normalization constants that are not affecting the CG procedure, such as the logarithm of the partition function.

Several methods have been proposed for defining a coarse-grained potential $U(\mathbf{x})$ that variationally approximates the consistency relation (3) at a particular thermodynamic state (temperature, pressure etc.) Two popular approaches are the multi-scale coarse-graining (force-matching)^{41,52} and the relative entropy method⁴³ (the two approaches are connected⁵³).

B. CG parameter estimation as a machine learning problem

Here we follow the force-matching scheme. It has been shown that thermodynamic consistency (2) is achieved when the CG model predicts the instantaneous CG forces with minimal mean error^{41,52}. We call the instantaneous atomistic forces $\mathbf{F}(\mathbf{r})$, and the instantaneous force projected on the CG coordinates $\xi(\mathbf{F}(\mathbf{r}))$. At the same time, the CG model predicts a force $-\nabla U(\mathbf{x}; \boldsymbol{\theta})$ for a CG configuration \mathbf{x} . The force matching error is defined as:

$$\chi^2(\boldsymbol{\theta}) = \left\langle \|\xi(\mathbf{F}(\mathbf{r})) + \nabla U(\xi(\mathbf{r}); \boldsymbol{\theta})\|^2 \right\rangle_{\mathbf{r}}. \quad (4)$$

The average $\langle \cdot \rangle_{\mathbf{r}}$ is over the equilibrium distribution of the atomistic model, i.e., $\mathbf{r} \sim \mu(\mathbf{r})$.

We reiterate a result shown in⁵² that has important consequences for using (4) in machine learning. For this, we introduce the mean force:

$$\mathbf{f}(\mathbf{x}) = \langle \xi(\mathbf{F}(\mathbf{r})) \rangle_{\mathbf{r}|\mathbf{x}} \quad (5)$$

where $\mathbf{r} | \mathbf{x}$ indicates the equilibrium distribution of \mathbf{r} constrained to the CG coordinates \mathbf{x} , i.e. the ensemble of all atomistic configurations that map to the same CG configuration. Then we can decompose expression (4) as follows (see SI for derivation):

$$\chi^2(\boldsymbol{\theta}) = \text{PMF error}(\boldsymbol{\theta}) + \text{Noise} \quad (6)$$

with the terms

$$\begin{aligned} \text{PMF error}(\boldsymbol{\theta}) &= \langle \|\mathbf{f}(\xi(\mathbf{r})) + \nabla U(\xi(\mathbf{r}); \boldsymbol{\theta})\|^2 \rangle_{\mathbf{r}} \\ \text{Noise} &= \langle \|\xi(\mathbf{F}(\mathbf{r})) - \mathbf{f}(\xi(\mathbf{r}))\|^2 \rangle_{\mathbf{r}}. \end{aligned} \quad (7)$$

This loss function differs from the force matching loss function used in the learning of force fields from quantum data by the Noise term. The Noise term is purely a function of the CG map ξ (and when training with finite simulation data also of the dataset), and it cannot be changed by varying the parameters $\boldsymbol{\theta}$. As a result, the total force matching error cannot be made zero but it is bounded from below by $\chi^2(\boldsymbol{\theta}) \geq \text{Noise}$ ⁵². On the contrary, when matching force fields from quantum data, the error χ^2 approaches zero for a sufficiently powerful model. Physically, the Noise term arises from the fact that instantaneous forces on the CG coordinates vary in the different atomistic configurations associated with the same CG configuration.

The learning problem is now to find a CG model and its parameters $\boldsymbol{\theta}$ that minimizes the PMF error term. In order to obtain a physical interpretation, we apply (1) and write the average purely in CG coordinates:

$$\begin{aligned} \text{PMF error}(\boldsymbol{\theta}) &= \langle \|\mathbf{f}(\mathbf{x}) + \nabla U(\mathbf{x}; \boldsymbol{\theta})\|^2 \rangle_{\mathbf{x}} \\ &= \langle \|\mathbf{f}(\mathbf{x}) - \hat{\mathbf{f}}(\mathbf{x}; \boldsymbol{\theta})\|^2 \rangle_{\mathbf{x}} \end{aligned}$$

This error term is the matching error between the mean force at the CG coordinates, $\mathbf{f}(\mathbf{x})$ and the CG forces predicted by the CG potential,

$$\hat{\mathbf{f}}(\mathbf{x}; \boldsymbol{\theta}) = -\nabla U(\mathbf{x}; \boldsymbol{\theta}). \quad (8)$$

Hence, the machine learning task is to find the free energy U whose negative derivatives are the mean forces, and U is thus called a potential of mean force (PMF). Eq. (8) implies that the mean force field $\hat{\mathbf{f}}$ is conservative, as it is generated by the free energy $U(\mathbf{x})$.

Machine learning the CG model is complicated by two aspects: (1) As the PMF error cannot be computed directly, its minimization in practice is accomplished by minimizing the variational bound (6). Thus, to learn $\mathbf{f}(\mathbf{x})$ accurately, we need to collect enough data “close” to every CG configuration \mathbf{x} such that the learning problem is dominated by the variations in the PMF error term and not by the variations in the Noise term. As a result, machine learning CG models typically requires more data points than force matching for potential energy surfaces; (2) The free energy $U(\mathbf{x})$ is not known a priori, but must be learned. In contrast to fitting potential energy surfaces we can therefore not directly use energies as inputs.

For a finite dataset $\mathbf{R} = (\mathbf{r}_1, \dots, \mathbf{r}_M)$ with M samples, we define the force matching loss function by the direct estimator:

$$L(\boldsymbol{\theta}; \mathbf{R}) = \frac{1}{M} \sum_{i=1}^M \|\xi(\mathbf{F}(\mathbf{r}_i)) + \nabla U(\xi(\mathbf{r}_i); \boldsymbol{\theta})\|^2 \quad (9)$$

$$= \|\xi(\mathbf{F}(\mathbf{R})) + \nabla U(\xi(\mathbf{R}); \boldsymbol{\theta})\|_F^2. \quad (10)$$

Where $\xi(\mathbf{R}) = [\xi(\mathbf{r}_1), \dots, \xi(\mathbf{r}_M)]^\top \in \mathbb{R}^{M \times 3n}$ and $\xi(\mathbf{F}(\mathbf{R})) = [\xi(\mathbf{F}(\mathbf{r}_1)), \dots, \xi(\mathbf{F}(\mathbf{r}_M))]^\top \in \mathbb{R}^{M \times 3n}$ are data matrices of coarse-grained coordinates and coarse-grained instantaneous forces that serve as an input to the learning method, and F denotes the Frobenius norm.

C. CG hyperparameter estimation as a machine learning problem

While Eq. (9) defines the training method, machine learning is not simply about fitting parameters for a given dataset, but rather about minimizing the expected prediction error (also called “risk”) for data not used for training. This concept is important in order to be able to select an optimal model, i.e. in order to choose the hyperparameters of the model, such as the type and number of neurons and layers in a neural network, or even to distinguish between different learning models such as a neural network and a spline model.

Statistical estimator theory is the field that studies optimal prediction errors⁵⁴. To compute the prediction error, we perform the following thought experiment: We consider the data \mathbf{R} as statistically independent realizations from the Boltzmann distribution,

$$\mathbf{r}_i \sim e^{-V(\mathbf{r}_i)/k_B T}.$$

This “ideal” scenario can only be approximated in practice, as \mathbf{R} is generated from MD or MCMC tra-

jectories that require many simulation steps before providing an independent sample. Following the argument, \mathbf{R} is a M -sample realization of the underlying Boltzmann distribution. The expected prediction error, or risk, $\mathbb{E}[L(\boldsymbol{\theta}; \mathbf{R})]$, is the expectation value over infinitely many repetitions of the following iteration:

1. Generate training set $\mathbf{R}^{\text{train}}$ and find $\hat{\boldsymbol{\theta}} = \arg \min_{\boldsymbol{\theta}} L(\boldsymbol{\theta}; \mathbf{R}^{\text{train}})$.
2. Generate test set \mathbf{R}^{test} and compute $L(\hat{\boldsymbol{\theta}}; \mathbf{R}^{\text{test}})$

where $\mathbf{R}^{\text{train}}$ and \mathbf{R}^{test} are two independent realizations. Although we cannot execute this thought experiment in practice, we can approximate it by cross-validation, and we can obtain insightful expressions for the form of the expected prediction error. As the loss function in force matching is a least squares regression problem, the form of the expected prediction error is well known (see SI for a short derivation), and can be written as:

$$\mathbb{E}[L(\boldsymbol{\theta}; \mathbf{R})] = \text{Bias}^2 + \text{Var} + \text{Noise} \quad (11)$$

with the Noise term as given in Eq. (7) and the bias and variance terms given by:

$$\text{Bias}^2 = \mathbb{E} \left[\|\mathbf{f}(\mathbf{R}) - \bar{\mathbf{f}}(\mathbf{R})\|_F^2 \right] \quad (12)$$

$$\text{Var} = \mathbb{E} \left[\|\bar{\mathbf{f}}(\mathbf{R}) + \nabla U(\xi(\mathbf{R}))\|_F^2 \right] \quad (13)$$

where

$$\bar{\mathbf{f}}(\mathbf{R}) = \mathbb{E}[-\nabla U(\xi(\mathbf{R}))]$$

is the mean estimator, i.e. the average force field learnt when the training is repeated many times for different data realizations. The terms in (12-13) have the following meaning: Eq. (12) is the expected error between the mean forces and the average predicted force field, it is therefore the systematic bias of the machine learning model. The variance (13) is the fluctuation of the individual estimates from single training procedures around the mean estimator and thus represents the estimator’s fluctuation due to finite-sample effects.

As the optimal model minimizes the PMF error, it must balance bias and variance. These contributions are typically counteracting: A too simple model (e.g., too small neural network) typically leads low variance but high bias, and it corresponds to “underfitting” the data. A too complex model (e.g., too large neural network) leads to low bias but large variance, and it corresponds to “overfitting” the data. The behavior of bias, variance and estimator error for a fixed data set size is illustrated in Fig. 1.

The optimum at which bias and variance balance depends on the amount of data used, and in the limit of an infinitely large dataset, the variance is zero and the optimal model can be made very complex so as to also make the bias zero. For small datasets, it is often favorable to reduce the model complexity and accept significant bias, in order to avoid large variance.

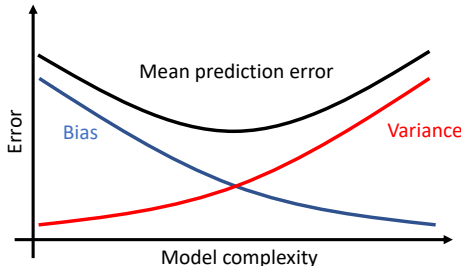


Figure 1. Typical bias-variance tradeoff for fixed data set size, indicating the balance between underfitting and overfitting.

In order to implement model selection, we approximate the “ideal” iteration above by the cross-validation method (algorithm 1 sketched below), and then choose the model or hyperparameter set that has the minimal cross-validation score.

Algorithm 1 Cross-validation

Cross-Validate(\mathbf{R} , L , K)

1. Split all available data into K approximately equal subsets: $\mathbf{R} = (\mathbf{R}^{(1)}, \dots, \mathbf{R}^{(K)})$
 2. For $k = 1, \dots, K$:
 - (a) $\mathbf{R}^{\text{train}} = \mathbf{R} \setminus \mathbf{R}^{(k)}$ (dataset without $\mathbf{R}^{(k)}$).
 - (b) Train: $\hat{\theta}_k = \arg \min_{\theta} L(\theta; \mathbf{R}^{\text{train}})$.
 - (c) Validation error: $L_k = L(\hat{\theta}_k; \mathbf{R}^{(k)})$
 3. Return cross-validation score $\frac{1}{K} \sum_{k=1}^K L_k$
-

D. CGnets: Learning CG force fields with neural networks

It is well known that the CG potential $U(\mathbf{x}; \theta)$ defined by thermodynamic consistency may be a complex multi-body potential even if the underlying atomistic potential has only few-body interactions⁵². To address this problem, we use artificial neural networks (ANNs) to represent $U(\mathbf{x}; \theta)$ as ANNs can approximate any smooth function on a bounded set of inputs, including multi-body functions⁵⁵.

Therefore, we use ANNs to model $U(\mathbf{x})$, train them by minimizing the loss (9) and select optimal models

by minimizing the cross-validation loss (Algorithm 1). For the purpose of training CG molecular models, we would like to have the following physical constraints and invariances, which determine parts of the architecture of the neural network:

- **Differentiable free energy function:** In order to train $U(\mathbf{x}; \theta)$ and simulate the associated dynamics by means of overdamped Langevin simulations, it must be differentiable. In order to simulate it by means of non-overdamped Langevin simulations, we need energy functions that are twice differentiable. As the present networks do not need to be very deep, vanishing gradients are not an issue and we select tanh activation functions here. After D nonlinear layers we always add one linear layer to map to one output neuron representing the free energy.
- **Translational and rotational invariance:** The energy of molecules that are not subject to an external field only depends on internal interactions and is invariant with respect to translation or rotation of the entire molecule. We therefore define a transformation:

$$\mathbf{y} = g(\mathbf{x})$$

from CG Cartesian coordinates \mathbf{x} to a set of features that contain the desired invariances, and use the features \mathbf{y} as an input to the network that computes the free energy, $U(g(\mathbf{x}); \theta)$. This transformation can be chosen in many different ways, e.g. by using local coordinate systems³⁴, two- or three-body correlation functions²⁰, or by a learnt representation²⁹. Here we choose the following features: distances between all pairs of CG atoms, the angles between three consecutive CG atoms, and the cos and sin of torsion angles defined by the CG atoms. The featurization layer is a nonparametric neural network layer.

- **Conservative PMF:** The PMF is a conservative force field generated by the free energy (8). As in quantum potential energy learning^{25,29}, we enforce this requirement by computing the free energy U with a neural network and then adding a gradient layer to compute the derivatives with respect to the input coordinates:

$$\hat{\mathbf{f}}(\mathbf{x}; \theta) = -\nabla_{\mathbf{x}} U(g(\mathbf{x}); \theta).$$

Fig. 2a shows the neural network architecture resulting from these choices. The free energy network is D layers deep and each layer is W neurons wide.

Thus, (D, W) are the remaining hyperparameters to be selected (as discussed in the Results section).

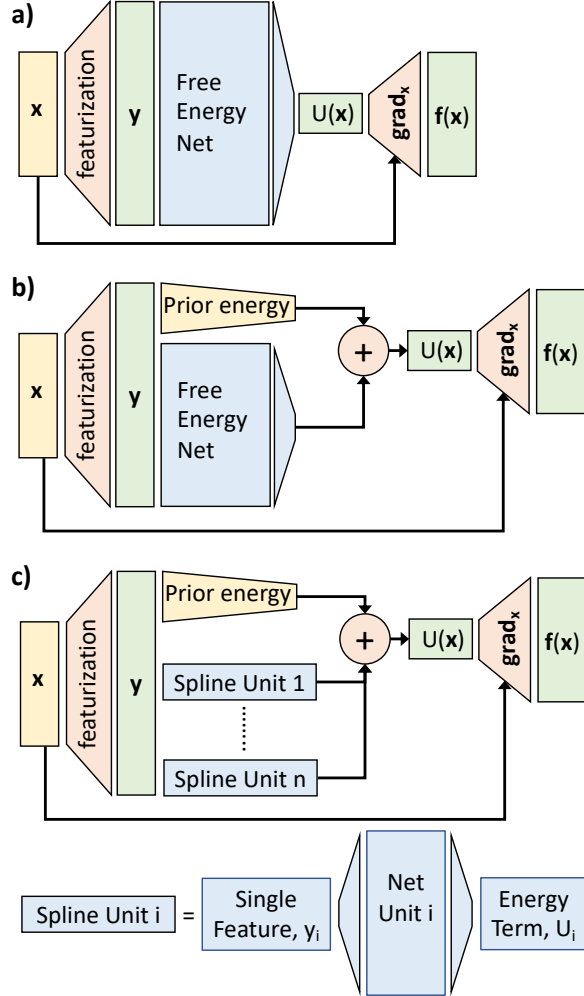


Figure 2. Neural network schemes. a) CGnet. b) Regularized CGnet with prior energy. c) Spline model representing a standard CG approach, for comparison. Each energy term is a function of only one feature, and the features are defined as all the bonds, angles, dihedrals, and nonbonded pairs of atoms.

E. Simulating the CGnet model

Once the neural network has been trained to produce a free energy $U(\mathbf{x})$, it can be used to simulate dynamical trajectories of the CG model. Here we use overdamped Langevin dynamics to advance the coordinates of the CG model from \mathbf{x}_t at time t to $\mathbf{x}_{t+\tau}$ after a timestep τ :

$$\mathbf{x}_{t+\tau} = \mathbf{x}_t - \tau \frac{D}{k_B T} \nabla U(\mathbf{x}_t) + \sqrt{2\tau D} \boldsymbol{\xi} \quad (14)$$

where \mathbf{x}_t is the CG configuration at time t (e.g., the x coordinate in the toy model and a 15-dimensional vector in the alanine dipeptide below). $\boldsymbol{\xi}$ is Gaussian random noise with zero mean and identity as covariance matrix, τ is the integration time step, D is the diffusion constant of the system. In the following, we use reduced energy units, i.e. all energies are in multiples of $k_B T$.

Since the implementation of CGnet is vectorized, it is more efficient to compute free energies and mean forces for an entire batch of configurations, rather than a single configuration at a time. Therefore, we run simulations in parallel for the examples shown below. This is done by sampling 100 starting points randomly from atomistic simulations, coarse-graining them and then integrating (14) stepwise.

F. Regularizing the free energy

Training the free energy with a network as shown in Fig. 2a and subsequently using it in order to simulate the dynamics with Eq. (14) produces trajectories of new CG coordinates \mathbf{x}_t . When parts of the coordinate space are reached that are very different from any point in the training set, it is possible that the network makes unphysical predictions.

In particular, the atomistic force-field used to produce the training data has terms that ensures the energy will go towards infinity when departing from physical states, e.g. when stretching bonds or when moving atoms too close to each other. These regions will not be sampled in the underlying MD simulations, and therefore result in “empty” parts of configuration space that contain no training data. Simulating a network trained only on physically valid training data via Eq. (14) may still produce points \mathbf{x}_t that enter this “forbidden regime” where bonds are overstretched or atoms start to overlap. At this point the simulation can become unstable if there is not regularizing effect ensuring that the predicted free energy $U(\mathbf{x}; \boldsymbol{\theta})$ will increase towards infinity when going deeper into the forbidden regime.

In order to avoid this problem, we introduce regularized CGnets (Fig. 2b). In a regularized CGnet, we define the energy function as

$$U(\mathbf{x}; \boldsymbol{\theta}) = U_0(\mathbf{x}) + U_{\text{net}}(\mathbf{x}; \boldsymbol{\theta}) \quad (15)$$

where $U_{\text{net}}(\mathbf{x}; \boldsymbol{\theta})$ is a neural network free energy as before and $U_0(\mathbf{x})$ is a prior energy that contains constraint terms that ensure basic physical behavior. Note that (15) can still be used to represent any smooth free energy because $U_{\text{net}}(\mathbf{x}; \boldsymbol{\theta})$ is a universal approximator. The role of $U_0(\mathbf{x})$ is to enforce $U \rightarrow \infty$ for unphysical states \mathbf{x} that are outside the

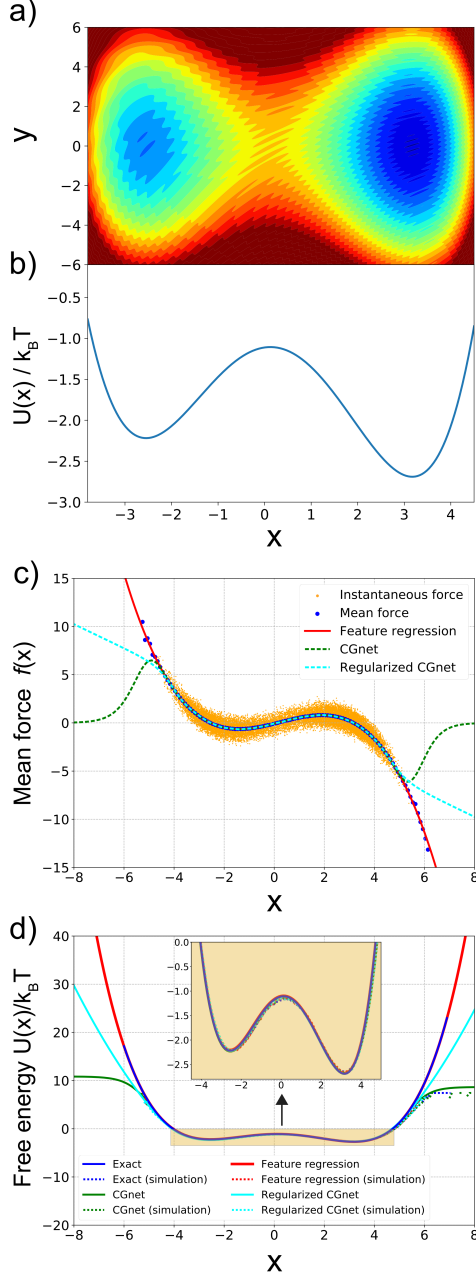


Figure 3. Machine-learned coarse-graining of dynamics in a rugged two-dimensional potential. (a) Two-dimensional potential used as toy system. (b) Exact free energy along x . (c) Instantaneous forces and the learned mean forces using feature regression and CGnet models (regularized and unregularized) compared to the exact forces. (d) Free energy (potential of mean force) along x predicted using least feature regression, and CGnet models compared to the exact free energy. Free energies are also computed from histogramming simulation data directly, using the underlying 2D trajectory, or simulations ran with the feature regression and CGnet models (dashed lines).

training data. Here, $U_0(\mathbf{x})$ is simply a sum of harmonic terms. For the 2d toy model, an harmonic term in the form $U_0(x) = \frac{1}{2}k(x - x_0)^2$ is used, and the parameters k and x_0 are determined by the force matching scheme restricted to the scarcely populated regions defined by the 100 sampled points with highest and the 100 with lowest x -value (see Fig. 3).

For alanine dipeptide, we use harmonic terms for the distance between atoms that are adjacent (connected by a covalent bonds) and for angles between three consecutive atoms. For each bond i , we use $U_{0,i}^{bond}(r_i; r_{i0}, k_{b,i}) = \frac{1}{2}k_{b,i}(r_i - r_{i0})^2$, where r_i is the instantaneous distance between the two consecutive atoms defining the bond, r_{i0} is the equilibrium bond length, and $k_{b,i}$ is a constant. Analogously, for each angle j , we use $U_{0,j}^{angle}(\theta_j; \theta_{j0}, k_{a,j}) = \frac{1}{2}k_{a,j}(\theta_j - \theta_{j0})^2$, where θ_j is the instantaneous value of the angle, θ_{j0} is the equilibrium value for the angle, and $k_{a,j}$ is a constant. When statistically independent, each such term would give rise to a Gaussian equilibrium distribution:

$$p(r_i) \propto \exp\left(-\frac{k_{b,i}(r_i - r_{i0})^2}{2k_B T}\right)$$

$$p(\theta_j) \propto \exp\left(-\frac{k_{a,j}(\theta_j - \theta_{j0})^2}{2k_B T}\right)$$

with mean $\mu = r_{i0}$ (or $\mu = \theta_{j0}$), and variance $\sigma^2 = k_B T/k_{b,i}$ (or $\sigma^2 = k_B T/k_{a,j}$). The prior energy is obtained by assuming independence between these energy terms and estimating these means and variances from the atomistic simulations. For larger molecules, we expect that additional terms need to be added that, e.g., penalize clashes between non-bonded atoms. We note that one could use classical CG approaches with predefined energy functions to first define the prior CG energy U_0 , then use an ANN to correct it with multi-body terms.

III. RESULTS

A. 2-dimensional toy model

As a simple illustration, we first present the results on the coarse-graining of a two-dimensional toy model. The potential energy is shown in Fig. 3 and given by the expression:

$$\frac{V(x, y)}{k_B T} = \frac{1}{50}(x - 4)(x - 2)(x + 2)(x + 3) + \frac{1}{20}y^2 + \frac{1}{25}\sin(3(x + 5)(y - 6)). \quad (16)$$

The potential corresponds to a double well along the x -axis and a harmonic confinement along the y -axis.

The last term in Eq. 16 adds small-scale fluctuations, appearing as small ripples in Fig. 3a.

The coarse-graining mapping is given by the projection of the 2-dimensional model onto the x -axis. In this simple toy-model, the coarse-grained free energy (potential of mean force) can be computed exactly (Fig. 3b):

$$\frac{U(x)}{k_B T} = -\log \left[\int_{-\infty}^{+\infty} \exp \left(-\frac{V(x, y)}{k_B T} \right) dy \right]$$

We generate a long (one million time steps) simulation trajectory of the 2-dimensional model and use the x component of the forces computed along the trajectories in the loss function 9. We report below the resulting CG potential obtained by 1) using a feature regression, i.e. least square regression with a set of feature functions defined in SI Section B, and 2) a CGnet (regularized and unregularized).

Cross-validation (Algorithm 1) is used to select the best hyperparameters for the least square regression and the CGnet architectures. For the feature regression, the same cross-validation procedure as introduced in⁵⁶ was used, and returned a linear combination of four basis functions among the selected set (see Fig. S1a and SI for details). For the regularized CGnet, a two stage cross-validation is conducted, first choosing the depth D with a fixed width of $W = 50$, and then choosing the width W (Fig. S1b, c). The minimal prediction error is obtained with $D = 1$ (one hidden layer) and $W = 50$. For the unregularized CGnet, a similar procedure is performed, and the best hyperparameters are selected as $D = 1, W = 120$.

Fig. 3c,d shows the results of the predicted mean forces and free energies (potential of mean force) in the x -direction. The instantaneous force fluctuates around the mean, but serves to accurately fit the exact mean force in the x range where sampling is abundant using both feature regression and CGnet (Fig. 3c). At the boundary where few samples are in the training data the predictors start to diverge from the exact mean force and free energy (Fig. 3c, d). This effect is more dramatic for the unregularized CGnet, in particular at large x values the CGnet makes an arbitrary prediction: here the force tends to zero. In the present example, reaching these states is highly improbable. However a CGnet simulation reaching this region can fail dramatically, as the simulation may continue to diffuse away from the low energy regime. As discussed above, this behavior can be avoided by adding a suitable prior energy that ensures that the free energy keeps increasing outside the training data, while not affecting the accuracy of the learn free energy within the training data (Fig. 3c, d). Note that the quantitative mismatch in the

low-probability regimes is not important for equilibrium simulations.

The matching mean forces translate into matching free energies (potentials of mean force, Fig. 3d). Finally, we conduct simulations with the learned models and generate trajectories $\{x_t\}$ using Eq. (14). From these, free energies can be computed by

$$\tilde{U}(\mathbf{x}) = -k_B T \log \tilde{p}_X(\mathbf{x}) \quad (17)$$

where $\tilde{p}_X(\mathbf{x})$ is a histogram estimate of the probability density of \mathbf{x} in the simulation trajectories. As shown in Fig. 3d, free energies agree well in the x range that has significant equilibrium probability.

B. Coarse-graining of alanine dipeptide in water

We now demonstrate CGnets on the coarse-graining of an all-atom MD simulation of alanine dipeptide in explicit solvent at $T = 300K$ to a simple model with 5 CG particles located at the five central backbone atoms of the molecule (Fig. 4). One trajectory of length 1 microsecond was generated using the simulation setup described in⁵⁷, coordinates and forces were saved every picosecond, giving rise to one million data points. The CG model has no solvent, therefore the CG procedure must learn the solvation free energy for all CG configurations.

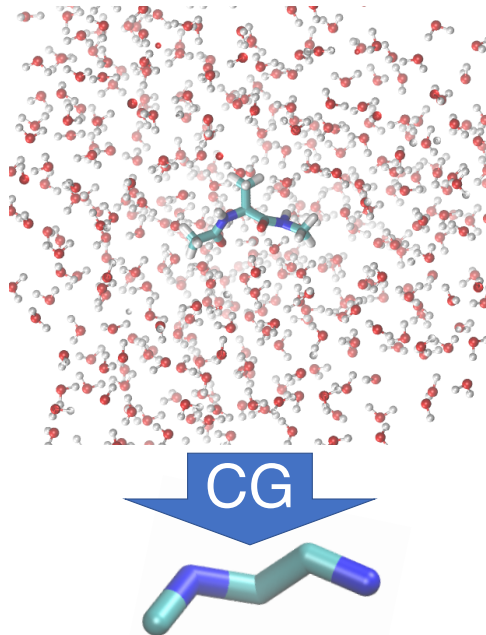


Figure 4. Mapping of alanine dipeptide from an all-atom solvated model (top) to a CG model consisting of the five central backbone atoms (bottom).

We compare two different CG models. The first model is defined by restricting the CG potential to a sum of terms that contain two-body interactions between nonbonded particles, and bonds, angles and dihedrals terms. We refer to this model as “spline model” in the following as it is analogous to the splines typically used in MD coarse-graining⁵⁸. This potential form is approximated by the “disconnected” network shown in Fig. 2c, i.e. we learn the spline for every pair interaction, bond, angle or dihedral, by using a neural network with a single input and output node.

The second model uses a regularized multi-body CGnet, i.e., a fully connected neural network shown in Fig. 2b to approximate the CG free energy. The comparison of the results from the two models allow us to evaluate the importance of multi-body interactions that are captured by the CGnet but are generally absent in CG models that use interaction terms involving a few atoms only.

The hyperparameters for both models consist of the number of layers (depth, D) and the number of neurons per layer (width, W) of the network, and are optimized by a two-stage cross-validation. In the first stage, we find the optimal D at fixed $W = 30$, subsequently we choose W at the optimal D . This results in $D = 3$ and $W = 60$ for CGnet, and $D = 4$ and $W = 50$ for the spline model (Fig. 5 and SI Section B). The cross-validation error of CGnet is significantly lower than the cross-validation error of the spline model (Fig. 5).

The selected models are used to generate CG MD simulation by iterating Eq. (14). For each model, one hundred independent simulations starting from structures sampled randomly from the atomistic simulation are performed for 1 million steps each, and the aggregated data are used to produce the free energy as a function of the dihedral coordinates. Fig. 6 compares the free energy computed via (17) from the underlying atomistic MD simulations and the free energy resulting from the two models. Only the regularized CGnet model can correctly reproduce the position of the all the main free energy minima (Fig. 6a, c). On the contrary, the spline model is not able to capture the shallow minima corresponding to positive values of the dihedral angle ϕ , and introduces several spurious minima (Fig. 6b). This comparison confirms that selecting CG models by minimal mean force prediction error achieves models that are better from a physical viewpoint.

For the CGnet, regularization is extremely important: without regularization the free energy only matches near the most pronounced minima and unphysical structures are sampled outside (Fig. 6d and SI Section D). With regularization, these unphysical

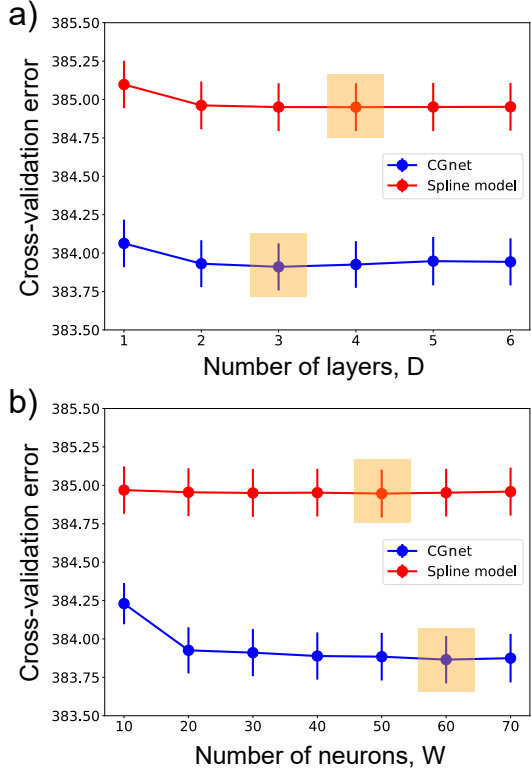


Figure 5. Top: cross validation for the selection of the network depth, D , for the regularized CGnet and the spline model. Middle: cross validation for the selection of the network width, W , for the two models. The selected hyperparameters with smallest cross-validation error are highlighted by orange boxes.

regimes are avoided, all sampled structures appear chemically valid (Fig. 6e) and the distributions of bonds and angles follow those in the atomistic simulations (SI Section D, Fig. S3).

IV. CONCLUSIONS

Here we have formulated coarse-graining based on the force-matching principle as a machine learning method. An important consequence of this formulation is that coarse-graining is a supervised learning problem whose loss function can be decomposed into the standard terms of statistical estimator theory: Bias, Variance and Noise. These terms have well-defined physical meanings and can be used in conjunction with cross-validation in order to select model hyperparameters and rank the quality of different coarse-graining models.

We have also introduced CGnets, a class of neural networks that can be trained with the force matching

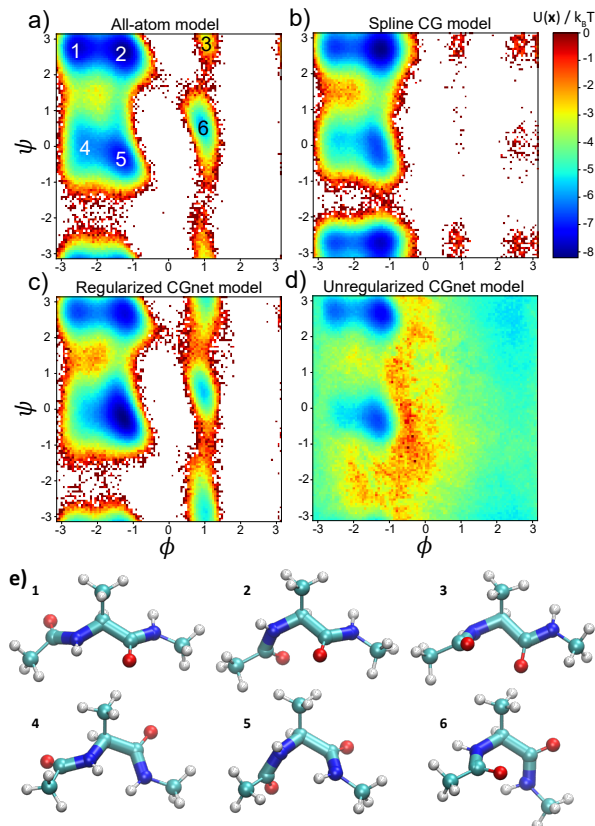


Figure 6. Free energy profiles and simulated structures of alanine dipeptide using all-atom and machine-learned coarse-grained models. (a) Reference free energy as a function of the dihedral angles, as obtained from direct histogram estimation from all-atom simulation. (b) Standard coarse-grained model using a sum of splines of individual internal coordinates. (c) Regularized CGnet as proposed here. (d) Unregularized CGnet. (e) Representative structures in the six free energy minima, from atomistic simulation (ball-and-stick representation) and regularized CGnet simulation (licorice representation).

principle and can encode all physically relevant invariances and constraints: (1) invariance of the free energy and mean force with respect to translation of the molecule, (2) invariance of the free energy and equivariance of the mean force with respect to rotation of the molecule, (3) the mean force is a conservative force field generated by the free energy, and (4) a prior energy can be applied in order to prevent the simulations with CGnets to diverge into unphysical state space regions outside the training data, such as states with overstretched bonds or clashing atoms.

The results presented above show that CGnet can be used to define effective energies for CG models that optimally reproduce the equilibrium distribution of a target atomistic model. CGnet provides a better approximation than functional forms com-

monly used for CG models as it automatically includes multi-body effects and non-linearities. The work presented here provides a proof of principle for this approach on simple systems. The extension to larger and more complex molecules presents additional challenges and may require to include additional terms to enforce physical constraints such as excluded volume.

Additionally, the CG model considered here is designed *ad hoc* for a specific molecule and is not transferable to the study of different systems. Transferability remains an outstanding issue in the design of coarse models¹¹ and its requirement may decrease the ability of reproducing faithfully properties of specific systems^{42,59–62}. In principle, transferable potentials can be obtained by designing input features for CGnet imposing a dependence of the energy function on the CG particle types and their environment⁶⁰, similarly to what is done in the learning of potential energy functions from quantum mechanics data (see e.g.^{20,24,27,33}). This approach may be able to define transferable functions if enough data are used in the training^{27,33}. We leave the investigation on the trade-off between transferability and accuracy for future studies.

It is also important to note that the formulation used here to define an optimal CG potential aims at reproducing structural properties of the system, but it does not determine the equations for its dynamical evolution. If one is interested in designing CG models that can reproduce molecular dynamical mechanisms, e.g. to reproduce the slow dynamical processes of the fine-grained model, alternative approaches need to be investigated.

REFERENCES

- ¹K. Lindorff-Larsen, S. Piana, R. O. Dror, and D. E. Shaw. How fast-folding proteins fold. *Science*, 334:517–520, 2011.
- ²I. Buch, M. J. Harvey, T. Giorgino, D. P. Anderson, and G. De Fabritiis. High-throughput all-atom molecular dynamics simulations using distributed computing. *J. Chem. Inf. Model.*, 50:397–403, 2010.
- ³M. Shirts and V. S. Pande. Screen savers of the world unite! *Science*, 290:1903–1904, 2000.
- ⁴R. O. Dror, A. C. Pan, D. H. Arlow, D. W. Borhani, P. Maragakis, Y. Shan, H. Xu, and D. E. Shaw. Pathway and mechanism of drug binding to g-protein-coupled receptors. *Proc. Natl. Acad. Sci. USA*, 108:13118–13123, 2011.
- ⁵D. Shukla, Y. Meng, B. Roux, and V. S. Pande. Activation pathway of src kinase reveals intermediate states as targets for drug design. *Nat. Commun.*, 5:3397, 2014.
- ⁶N. Plattner and F. Noé. Protein conformational plasticity and complex ligand binding kinetics explored by atomistic simulations and markov models. *Nat. Commun.*, 6:7653, 2015.
- ⁷N. Plattner, S. Doerr, G. D. Fabritiis, and F. Noé. Protein-

- protein association and binding mechanism resolved in atomic detail. *Nat. Chem.*, 9:1005–1011, 2017.
- ⁸F. Paul, C. Wehmeyer, E. T. Abualrous, H. Wu, M. D. Crabtree, J. Schöneberg, J. Clarke, C. Freund, T. R. Weikl, and F. Noé. Protein-ligand kinetics on the seconds timescale from atomistic simulations. *Nat. Commun.*, 8:1095, 2017.
 - ⁹C. Clementi. Coarse-grained models of protein folding: Toy-models or predictive tools? *Curr. Opin. Struct. Biol.*, 18:10–15, 2008.
 - ¹⁰M. G. Saunders and G. A. Voth. Coarse-graining methods for computational biology. *Annu. Rev. Biophys.*, 42(1):73–93, 2013.
 - ¹¹W. G. Noid. Perspective: Coarse-grained models for biomolecular systems. *J. Chem. Phys.*, 139(9):090901, 2013.
 - ¹²S. Matysiak and C. Clementi. Optimal combination of theory and experiment for the characterization of the protein folding landscape of s6: How far can a minimalist model go? *J. Mol. Biol.*, 343:235–248, 2004.
 - ¹³S. Matysiak and C. Clementi. Minimalist protein model as a diagnostic tool for misfolding and aggregation. *J. Mol. Biol.*, 363:297–308, 2006.
 - ¹⁴J. Chen, J. Chen, G. Pinamonti, and C. Clementi. Learning effective molecular models from experimental observables. *J. Chem. Theory Comput.*, 14(7):3849–3858, 2018.
 - ¹⁵A. Mardt, L. Pasquali, H. Wu, and F. Noé. Vampnets: Deep learning of molecular kinetics. *Nat. Commun.*, 9:5, 2018.
 - ¹⁶H. Wu, A. Mardt, L. Pasquali, and F. Noé. Deep generative markov state models. *NIPS (in press). Preprint: arXiv:1805.07601*, 2018.
 - ¹⁷C. Wehmeyer and F. Noé. Time-lagged autoencoders: Deep learning of slow collective variables for molecular kinetics. *J. Chem. Phys.*, 148:241703, 2018.
 - ¹⁸C. X. Hernández, H. K. Wayment-Steele, M. M. Sultan, B. E. Husic, and V. S. Pande. Variational encoding of complex dynamics. *arXiv:1711.08576*, 2017.
 - ¹⁹J. M. L. Ribeiro, P. Bravo, Y. Wang, and P. Tiwary. Reweighted autoencoded variational bayes for enhanced sampling (rave). *J. Chem. Phys.*, 149:072301, 2018.
 - ²⁰J. Behler and M. Parrinello. Generalized neural-network representation of high-dimensional potential-energy surfaces. *Phys. Rev. Lett.*, 98:146401, 2007.
 - ²¹A. P. Bartók, M. C. Payne, R. Kondor, and G. Csányi. Gaussian approximation potentials: The accuracy of quantum mechanics, without the electrons. *Phys. Rev. Lett.*, 104(13), 2010.
 - ²²M. Rupp, A. Tkatchenko, K.-R. Müller, and O. A. von Lilienfeld. Fast and accurate modeling of molecular atomization energies with machine learning. *Phys. Rev. Lett.*, 108(5), 2012.
 - ²³A. P. Bartók, M. J. Gillan, F. R. Manby, and G. Csányi. Machine-learning approach for one- and two-body corrections to density functional theory: Applications to molecular and condensed water. *Phys. Rev. B*, 88(5), 2013.
 - ²⁴J. S. Smith, O. Isayev, and A. E. Roitberg. ANI-1: an extensible neural network potential with DFT accuracy at force field computational cost. *Chem. Sci.*, 8(4):3192–3203, 2017.
 - ²⁵S. Chmiela, A. Tkatchenko, H. E. Sauceda, I. Poltavsky, K. T. Schütt, and K.-R. Müller. Machine learning of accurate energy-conserving molecular force fields. *Sci. Adv.*, 3(5), 2017.
 - ²⁶A. P. Bartók, S. De, C. Poelking, N. Bernstein, J. R. Kermode, G. Csányi, and M. Ceriotti. Machine learning unifies the modeling of materials and molecules. *Sci. Adv.*, 3(12), 2017.
 - ²⁷K. T. Schütt, F. Arbabzadah, S. Chmiela, K. R. Müller, and A. Tkatchenko. Quantum-chemical insights from deep tensor neural networks. *Nat. Commun.*, 8:13890, 2017.
 - ²⁸J. S. Smith, B. Nebgen, N. Lubbers, O. Isayev, and A. E. Roitberg. Less is more: Sampling chemical space with active learning. *J. Chem. Phys.*, 148(24):241733, 2018.
 - ²⁹K. T. Schütt, H. E. Sauceda, P.-J. Kindermans, A. Tkatchenko, and K.-R. Müller. SchNet - a deep learning architecture for molecules and materials. *J. Chem. Phys.*, 148(24):241722, 2018.
 - ³⁰A. Grisafi, D. M. Wilkins, G. Csányi, and M. Ceriotti. Symmetry-adapted machine learning for tensorial properties of atomistic systems. *Phys. Rev. Lett.*, 120(3), 2018.
 - ³¹G. Imbalzano, A. Anelli, D. Gíofré, S. Klees, J. Behler, and M. Ceriotti. Automatic selection of atomic fingerprints and reference configurations for machine-learning potentials. *J. Chem. Phys.*, 148(24):241730, 2018.
 - ³²T. T. Nguyen, E. Székely, G. Imbalzano, J. Behler, G. Csányi, M. Ceriotti, A. W. Götz, and F. Paesani. Comparison of permutationally invariant polynomials, neural networks, and gaussian approximation potentials in representing water interactions through many-body expansions. *J. Chem. Phys.*, 148(24):241725, 2018.
 - ³³L. Zhang, J. Han, H. Wang, W. A. Saidi, R. Car, and W. E. End-to-end symmetry preserving inter-atomic potential energy model for finite and extended systems. *arXiv:1805.09003*, 2018.
 - ³⁴L. Zhang, J. Han, H. Wang, R. Car, and W. E. Deep potential molecular dynamics: a scalable model with the accuracy of quantum mechanics. *Phys. Rev. Lett.*, 120:143001, 2018.
 - ³⁵T. Bereau, R. A. DiStasio, A. Tkatchenko, and O. A. V. Lilienfeld. Non-covalent interactions across organic and biological subsets of chemical space: Physics-based potentials parametrized from machine learning. *J. Chem. Phys.*, 148:241706, 2018.
 - ³⁶S. T. John and G. Csányi. Many-body coarse-grained interactions using gaussian approximation potentials. *J. Phys. Chem. B*, 121(48):10934–10949, 2017.
 - ³⁷L. Zhang, J. Han, H. Wang, R. Car, and W. E. DeePCG: constructing coarse-grained models via deep neural networks. *arXiv:1802.08549*, 2018.
 - ³⁸A. P. Lyubartsev and A. Laaksonen. Calculation of effective interaction potentials from radial distribution functions: A reverse monte carlo approach. *Phys. Rev. E*, 52(4):3730–3737, 1995.
 - ³⁹F. Müller-Plathe. Coarse-graining in polymer simulation: From the atomistic to the mesoscopic scale and back. *ChemPhysChem*, 3(9):754–769, sep 2002.
 - ⁴⁰M. Praprotnik, L. D. Site, and K. Kremer. Multiscale simulation of soft matter: From scale bridging to adaptive resolution. *Ann. Rev. Phys. Chem.*, 59(1):545–571, 2008.
 - ⁴¹S. Izvekov and G. A. Voth. A multiscale coarse-graining method for biomolecular systems. *J. Phys. Chem. B*, 109(7):2469–2473, 2005.
 - ⁴²Y. Wang, W. G. Noid, P. Liu, and G. A. Voth. Effective force coarse-graining. *Phys. Chem. Chem. Phys.*, 11(12):2002, 2009.
 - ⁴³M. S. Shell. The relative entropy is fundamental to multiscale and inverse thermodynamic problems. *J. Phys. Chem.*, 129(14):144108, 2008.
 - ⁴⁴C. Clementi, H. Nymeyer, and J. N. Onuchic. Topological and energetic factors: what determines the structural details of the transition state ensemble and “en-route” intermediates for protein folding? Investigation for small globular proteins. *J. Mol. Biol.*, 298(5):937–953, 2000.
 - ⁴⁵S. O. Nielsen, C. F. Lopez, G. Srinivas, and M. L. Klein. A coarse grain model for n-alkanes parameterized from surface tension data. *J. Chem. Phys.*, 119(14):7043–7049, 2003.
 - ⁴⁶S. J. Marrink, A. H. de Vries, and A. E. Mark. Coarse

- grained model for semiquantitative lipid simulations. *J. Phys. Chem. B*, 108(2):750–760, 2004.
- ⁴⁷A. Davtyan, N. P. Schafer, W. Zheng, C. Clementi, P. G. Wolynes, and G. A. Papoian. AWSEM-MD: Protein structure prediction using coarse-grained physical potentials and bioinformatically based local structure biasing. *J. Phys. Chem. B*, 116(29):8494–8503, 2012.
- ⁴⁸G. A. Voth. *Coarse-graining of condensed phase and biomolecular systems*. CRC press, 2008.
- ⁴⁹L. Monticelli, S. K. Kandasamy, X. Periole, R. G. Larson, D. P. Tieleman, and S.-J. Marrink. The MARTINI coarse-grained force field: Extension to proteins. *J. Chem. Theory Comput.*, 4(5):819–834, 2008.
- ⁵⁰A. V. Sinititskiy, M. G. Saunders, and G. A. Voth. Optimal number of coarse-grained sites in different components of large biomolecular complexes. *J. Phys. Chem. B*, 116(29):8363–8374, 2012.
- ⁵¹L. Boninsegna, R. Banisch, and C. Clementi. A data-driven perspective on the hierarchical assembly of molecular structures. *J. Chem. Theory Comput.*, 14(1):453–460, 2018.
- ⁵²W. G. Noid, J.-W. Chu, G. S. Ayton, V. Krishna, S. Izvekov, G. A. Voth, A. Das, and H. C. Andersen. The multiscale coarse-graining method. I. A rigorous bridge between atomistic and coarse-grained models. *J. Chem. Phys.*, 128(24):244114, 2008.
- ⁵³J. F. Rudzinski and W. G. Noid. Coarse-graining entropy, forces, and structures. *J. Phys. Chem.*, 135(21):214101, 2011.
- ⁵⁴V. N. Vapnik. An overview of statistical learning theory. *IEEE Trans. Neur. Net.*, 10, 1999.
- ⁵⁵K. Hornik. Approximation capabilities of multilayer feed-forward networks. *Neural Networks*, 4:251–257, 1991.
- ⁵⁶L. Boninsegna, F. Nüske, and C. Clementi. Sparse learning of stochastic dynamical equations. *J. Chem. Phys.*, 148(24):241723, jun 2018.
- ⁵⁷F. Nüske, H. Wu, C. Wehmeyer, C. Clementi, and F. Noé. Markov state models from short non-equilibrium simulations - analysis and correction of estimation bias. *J. Chem. Phys.*, 146:094104, 2017.
- ⁵⁸N. J. H. Dunn, K. M. Lebold, M. R. DeLyser, J. F. Rudzinski, and W. Noid. BOCS: Bottom-up open-source coarse-graining software. *J. Phys. Chem. B*, 122(13):3363–3377, 2017.
- ⁵⁹M. E. Johnson, T. Head-Gordon, and A. A. Louis. Representability problems for coarse-grained water potentials. *J. Chem. Phys.*, 126(14):144509, 2007.
- ⁶⁰J. W. Mullinax and W. G. Noid. Extended ensemble approach for deriving transferable coarse-grained potentials. *J. Chem. Phys.*, 131(10):104110, 2009.
- ⁶¹I. F. Thorpe, D. P. Goldenberg, and G. A. Voth. Exploration of transferability in multiscale coarse-grained peptide models. *J. Phys. Chem. B*, 115(41):11911–11926, 2011.
- ⁶²E. C. Allen and G. C. Rutledge. Evaluating the transferability of coarse-grained, density-dependent implicit solvent models to mixtures and chains. *J. Chem. Phys.*, 130(3):034904, 2009.
- ⁶³D. P. Kingma and J. Ba. Adam: A method for stochastic optimization. *arXiv:1412.6980*, 2014.

SUPPLEMENTARY MATERIAL

A. Decomposition of the force matching error

The decomposition of the force matching error (4) can be achieved by adding and subtracting the mean force (5) and splitting the norm:

$$\begin{aligned}\chi^2 [U(\mathbf{x})] &= \left\langle \left\langle \|\xi(\mathbf{F}(\mathbf{r})) - \mathbf{f}(\mathbf{x}) + \mathbf{f}(\mathbf{x}) + \nabla U(\mathbf{x})\|^2 \right\rangle_{\mathbf{r}|\mathbf{x}} \right\rangle_{\mathbf{x}} \\ &= \left\langle \left\langle \|\xi(\mathbf{F}(\mathbf{r})) - \mathbf{f}(\mathbf{x})\|^2 \right\rangle_{\mathbf{r}|\mathbf{x}} \right\rangle_{\mathbf{x}} + \left\langle \|\mathbf{f}(\mathbf{x}) + \nabla U(\mathbf{x})\|^2 \right\rangle_{\mathbf{x}} \\ &\quad + 2 \left\langle \left\langle (\xi(\mathbf{F}(\mathbf{r})) - \mathbf{f}(\mathbf{x}))^\top (\mathbf{f}(\mathbf{x}) + \nabla U(\mathbf{x})) \right\rangle_{\mathbf{r}|\mathbf{x}} \right\rangle_{\mathbf{x}}.\end{aligned}$$

This expression is equivalent to Eq. (6). as the mixed term is zero:

$$\begin{aligned}&\left\langle \left\langle (\xi(\mathbf{F}(\mathbf{r})) - \mathbf{f}(\mathbf{x}))^\top (\mathbf{f}(\mathbf{x}) + \nabla U(\mathbf{x})) \right\rangle_{\mathbf{r}|\mathbf{x}} \right\rangle_{\mathbf{x}} \\ &= \langle \mathbf{f}(\mathbf{x})^\top \mathbf{f}(\mathbf{x}) \rangle_{\mathbf{x}} + \langle \mathbf{f}(\mathbf{x})^\top \nabla U(\mathbf{x}) \rangle_{\mathbf{x}} \\ &\quad - \langle \mathbf{f}(\mathbf{x})^\top \mathbf{f}(\mathbf{x}) \rangle_{\mathbf{x}} - \langle \mathbf{f}(\mathbf{x})^\top \nabla U(\mathbf{x}) \rangle_{\mathbf{x}} \\ &= 0\end{aligned}$$

The decomposition of the expected prediction error in the form of Eq. 11 can be achieved by adding and subtracting the mean estimator $\bar{U} = \mathbb{E} [\nabla U(\xi(\mathbf{R}); \boldsymbol{\theta})]$:

$$\begin{aligned}\mathbb{E} [L(\boldsymbol{\theta}; \mathbf{R})] &= \mathbb{E} \left[\|\xi(\mathbf{F}(\mathbf{R})) + \nabla U(\xi(\mathbf{R}); \boldsymbol{\theta})\|_F^2 \right] \\ &= \mathbb{E} \left[\left\| \underbrace{\xi(\mathbf{F}(\mathbf{R})) - \bar{U}}_a + \underbrace{\bar{U} + \nabla U(\xi(\mathbf{R}); \boldsymbol{\theta})}_b \right\|_F^2 \right] \\ &= \mathbb{E} [a^2] + \mathbb{E} [b^2] + 2\mathbb{E} [ab]\end{aligned}$$

We follow standard results for regression. The mixed term disappears:

$$\begin{aligned}\mathbb{E} [ab] &= \mathbb{E} \left[(\xi(\mathbf{F}(\mathbf{R})) - \bar{U})^\top (\bar{U} + \nabla U(\xi(\mathbf{R}); \boldsymbol{\theta})) \right] \\ &= \mathbb{E} [\xi(\mathbf{F}(\mathbf{R}))^\top] \bar{U} + \mathbb{E} [\xi(\mathbf{F}(\mathbf{R}))^\top \nabla U(\xi(\mathbf{R}); \boldsymbol{\theta})] - \mathbb{E} [\bar{U}^\top \bar{U}] - \bar{U}^\top \mathbb{E} [\nabla U(\xi(\mathbf{R}); \boldsymbol{\theta})] \\ &= 0.\end{aligned}$$

B. Cross-validation of the CG models

We report there the results from cross-validation for the choice of hyperparameters of all models discussed in the main text.

The feature regression for the coarse-graining of the 2 dimensional toy model is performed with the twenty basis functions listed in Table S1 selected as features. Cross-validation is performed with the Stepwise Sparse Regressor introduced in⁵⁶. The minimum cross-validation error is obtained when the first four functions are used as features.

The results for the CGnet for the toy 2 dimensional system are reported in Tables S2 and S3, and for the coarse graining of alanine dipeptide in Table S4, both for CGnet and the spline model.

Table S1. Twenty elementary basis functions.

function ID	function, $f(x)$	function ID	function, $f(x)$
1	1	11	x^{10}
2	x	12	$\sin(x)$
3	x^2	13	$\cos(x)$
4	x^3	14	$\sin(6x)$
5	x^4	15	$\cos(6x)$
6	x^5	16	$\sin(11x)$
7	x^6	17	$\cos(11x)$
8	x^7	18	$\tanh(10x)$
9	x^8	19	$\tanh^2(10x)$
10	x^9	20	e^{-50x^2}

Table S2. Hyperparameter optimization for unregularized CGnet of two-dimensional model system. D : network depth, W : network width.

D	Cross-validation error	W	Cross-validation error
1	946.137 \pm 6.123	5	1418.483 \pm 10.966
2	1364.261 \pm 243.215	10	2190.571 \pm 12.005
3	1834.791 \pm 74.624	20	946.137 \pm 6.123
4	1423.804 \pm 42.916	40	932.235 \pm 4.264
5	2135.871 \pm 306.791	60	925.676 \pm 3.254
		80	920.471 \pm 3.359
		100	917.853 \pm 3.296
		120	915.196 \pm 2.931
		150	915.360 \pm 2.917

Table S3. Hyperparameter optimization for regularized CGnet of two-dimensional model system. D : network depth, W : network width.

D	Cross-validation error	W	Cross-validation error
1	914.300 \pm 2.634	5	3956.454 \pm 7.593
2	920.283 \pm 2.495	10	1472.033 \pm 7.384
3	924.625 \pm 4.055	20	924.642 \pm 3.760
4	931.437 \pm 3.980	50	914.300 \pm 2.634
5	931.965 \pm 3.877	80	914.742 \pm 2.530
		100	915.583 \pm 2.387
		120	915.246 \pm 2.533
		150	916.355 \pm 2.441
		200	916.625 \pm 2.379
		300	917.366 \pm 2.488

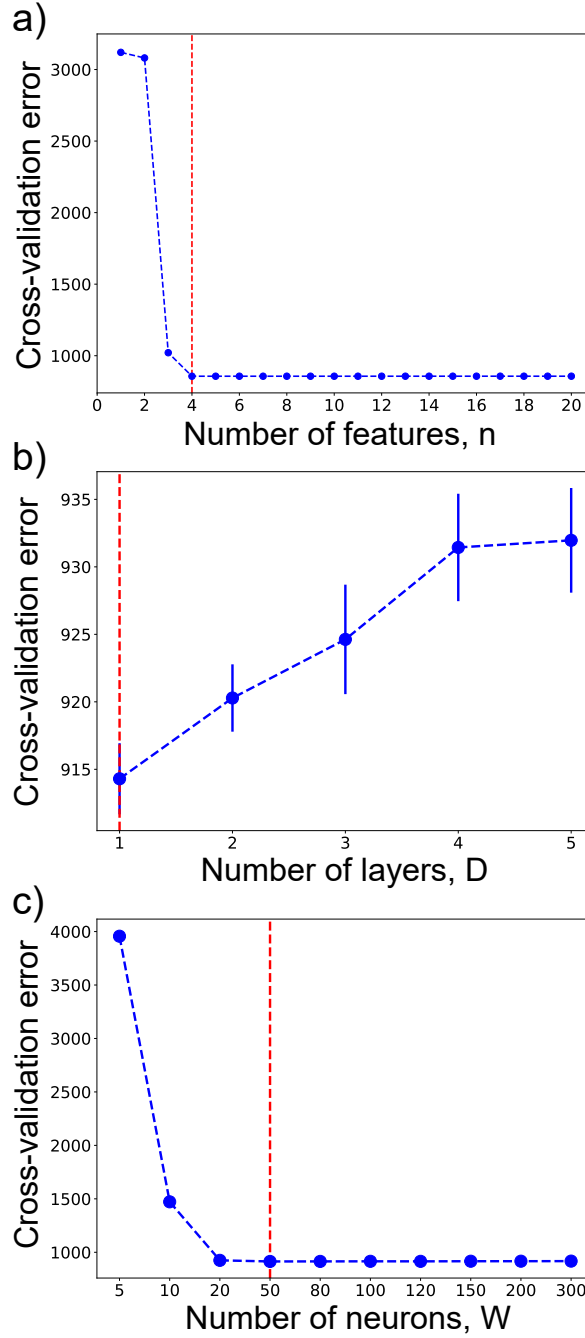


Figure S1. Model selection for CG model of 2D system using cross-validation. a) Choice of the set of feature functions for feature regression. b) First stage of regularized CGnet hyperparameter selection: the optimal number of layers, D . c). Second stage of regularized CGnet hyperparameter selection: the optimal number of neurons per layer, W . Red dashed lines indicate the minimal cross-validation error. Error bars represent the standard error of the mean 'Cross-validation error' over five cross-validation folds, in panels a) and c) the error bars are invisible as they are smaller than the marker.

Table S4. Hyperparameter optimization for regularized CGnet and spline model of alanine dipeptide. Left: network depth D , right: network width W . The uncertainty represents the standard error of the mean, $\sigma/\sqrt{5}$, where σ is the standard deviation of the validation error from five validation folds. The best model, corresponding to the smallest cross validation error, is highlighted.

D	CGnet	Spline model	W	CGnet	Spline model
1	384.063 \pm 0.155	385.098 \pm 0.154	10	384.230 \pm 0.134	384.969 \pm 0.154
2	383.931 \pm 0.153	384.962 \pm 0.156	20	383.926 \pm 0.150	384.955 \pm 0.156
3	383.911 \pm 0.153	384.951 \pm 0.156	30	383.911 \pm 0.153	384.950 \pm 0.156
4	383.926 \pm 0.152	384.950 \pm 0.156	40	383.889 \pm 0.154	384.952 \pm 0.155
5	383.948 \pm 0.157	384.952 \pm 0.156	50	383.884 \pm 0.155	384.946 \pm 0.156
6	383.943 \pm 0.153	384.952 \pm 0.155	60	383.865 \pm 0.154	384.952 \pm 0.155
			70	383.875 \pm 0.158	384.958 \pm 0.156

C. Training CG models

Networks were optimized using the Adam adaptive stochastic gradient descent method⁶³ with default settings using the PyTorch program. The batchsize was 128 for the 2D model and 512 for alanine dipeptide. The convergence of the training error and validation error for the 2d toy model and alanine dipeptide is shown in Fig. S2 below.

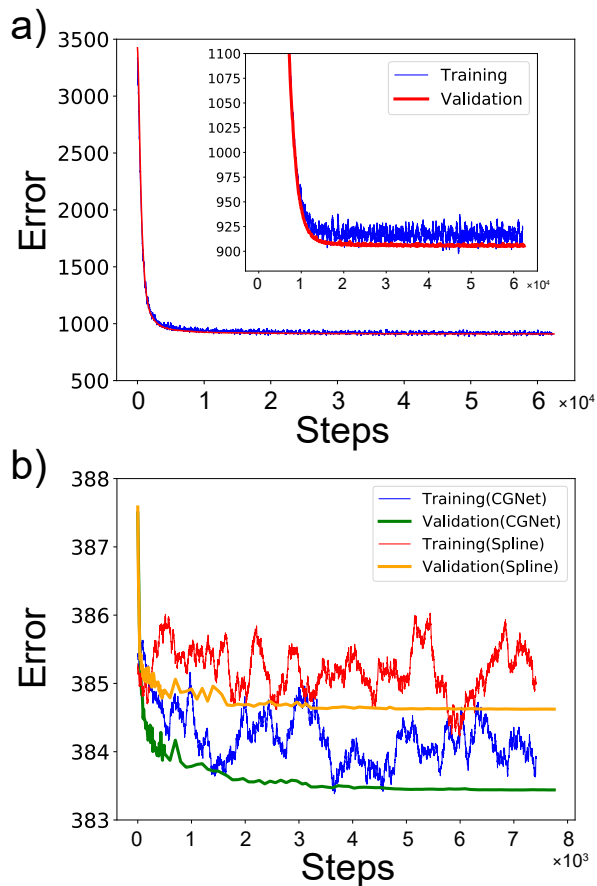


Figure S2. Training error and validation error for (a) the 2D model and (b) alanine dipeptide. In (a), the model is the regularized CGnet, in (b), the model is the regularized CGnet and the spline model, which is also regularized. All errors are averaged over 200000 points – for the training error this is done by averaging over the most recent batches, while the validation error is shown for a fixed validation set. Note that the hyperparameter choices are made via cross-validation.

D. Distribution of bond distances and angles for the different models of alanine dipeptide

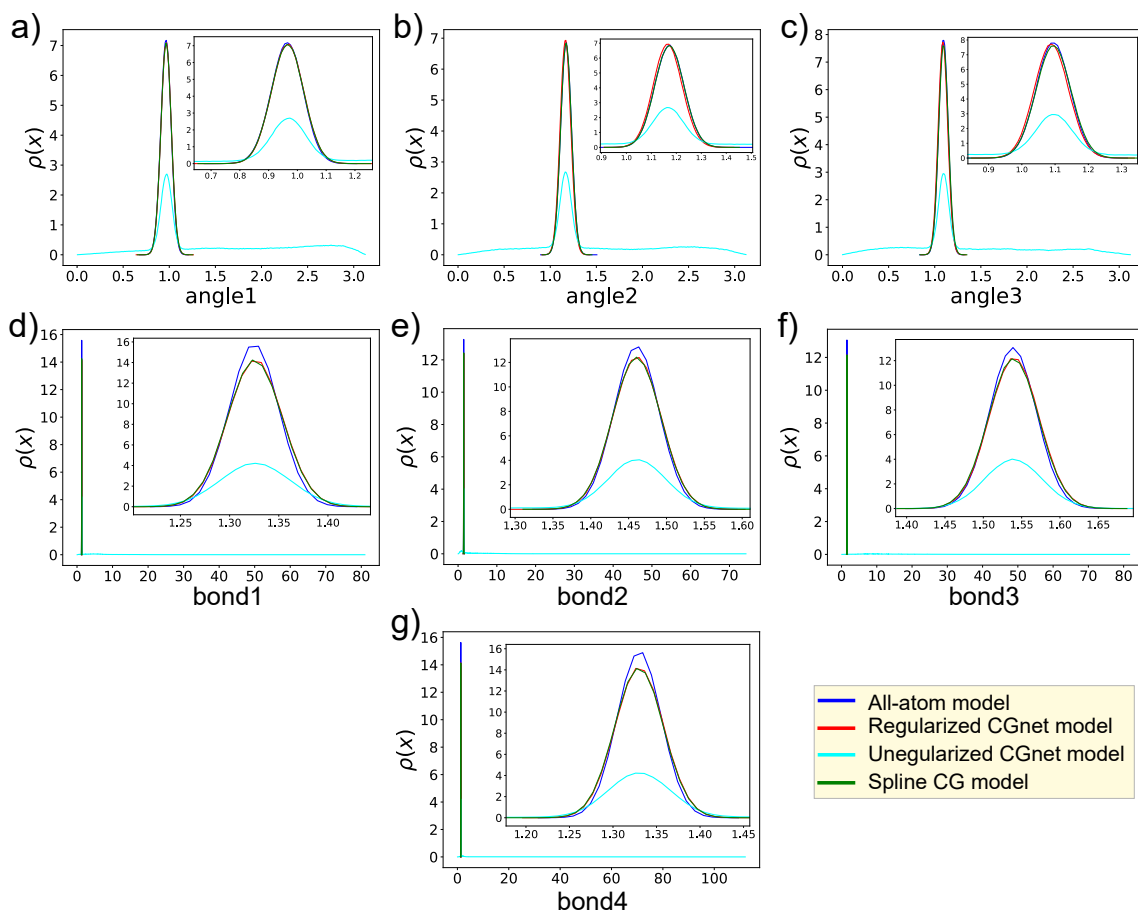


Figure S3. Probability density distribution for three angles a)- c), and four bonds d)-g). Each panel contains the distribution from four models: All-atom model (blue), regularized CGnet model (red), unregularized CGnet model (cyan), spline CG model (green). The distribution for regularized CGnet and spline model (with regularization) agree with the true all-atom one. The distribution for the unregularized CGnet has a wide range, which makes the distributions for the other models appear very narrow in d)-g). The insets in d)-g) present zoomed views of the distributions in the correct range.